Mineral dust plume evolution over the Atlantic from MISR and MODIS aerosol retrievals

Olga V. Kalashnikova[1] and Ralph A. Kahn[2]

Received 6 March 2008; revised 9 June 2008; accepted 14 August 2008; published 19 December 2008.

[1] We demonstrate how Multiangle Imaging Spectroradiometer (MISR) and Moderate Resolution Imaging Spectroradiometer (MODIS) space-based aerosol products provide complementary information, characterizing (1) transported desert dust plume extent over water, (2) aerosol optical thickness (AOT) evolution, and (3) particle size sensitivity and fraction spherical evolution for the thicker parts of these plumes. MODIS provides more extensive coverage, whereas MISR's multiangle retrievals include dust properties and fill in areas where glint precludes MODIS optical depth retrievals, increasing by up to 50% dust plume surface area coverage compared to MODIS-only observations. These results can be used to improve dust aerosol representations in climate, forecast, and transport models. Extensive comparison of MISR and MODIS AOT retrievals with Aerosol Robotic Network (AERONET) observations in dusty regions show accuracies of about 20%; MISR Angstrom exponent is predominantly less than 1, in reasonably good agreement with AERONET. For four selected North African dust transport events, combined MISR and MODIS observations map systematic changes in retrieved plume surface area, on the basis of AOT contours; these reflect differences in aerosol dispersion and removal rates that must be reproduced by models. Within MISR retrieval uncertainties, Angstrom exponent and AOT fraction spherical are lower in the optically thicker parts of the plume by up to 30% and increase as the plume is transported across the ocean, as would be expected; retrieved single-scattering albedo values are ~0.98 for all stages of plume evolution. For the cases studied, AERONET shows similar property patterns at points on either side of the Atlantic and indicates ~15% decrease in aerosol coarse mode effective radius during transoceanic transport.

Citation: Kalashnikova, O. V., and R. A. Kahn (2008), Mineral dust plume evolution over the Atlantic from MISR and MODIS aerosol retrievals, *J. Geophys. Res.*, *113*, D24204, doi:10.1029/2008JD010083.

1. Introduction

[2] Mineral dust particles have significant effects on the climate and the environment, and despite notable advances in modeling, satellite observation, and ground-based measurements, they remain the dominant factor in the uncertainty of radiative forcing [*Yu et al.*, 2006; *Mishchenko et al.*, 2007]. Dust particles transported over the ocean affect marine biochemistry by depositing iron in the ocean [*Martin et al.*, 1991; *Bopp et al.*, 2003], play a role in neutralizing acid rain [*Wang et al.*, 2002], affect the life cycle of coral reefs [*Shinn et al.*, 2000] and influence sea surface temperatures that impact hurricane formation and intensity [*Evan et al.*, 2006; *Wu*, 2007]. Current estimates of dust emission and deposition uncertainty vary by an order of magnitude in some regions, because of the high spatial and temporal variability of the field itself, and limited observations [*Mahowald et al.*, 2005]. Recently available NASA satellite data from next-generation sensors (Table 1) make it possible to improve model predictions by providing significant new information about dust emission, transport, deposition, and property evolution, through dust radiative signatures.

[3] The TOMS aerosol index (AI) has been used for dust source characterization [*Prospero et al.*, 2002] and for monitoring dust transport interannual variability [*Chiapello et al.*, 2005]. Moderate Resolution Imaging Spectroradiometer (MODIS) aerosol optical thickness (AOT) data were used to estimate the cross-Atlantic flux and deposition budget of Saharan dust, on the basis of the AOT–westward wind correlation [*Kaufman et al.*, 2005]. MODIS AOT and AIRS temperature data were compared with model simulations to reveal interactions between large-scale meteorological fields and the intercontinental transport of the Saharan Air Layer (SAL) [*Wong et al.*, 2006]. Some dust plume properties, such as dust altitude, infrared optical thickness and effective particle size, can be retrieved from AIRS data [*Pierangelo et al.*, 2004, 2005]. MODIS and TOMS observations were also used to validate the dust transports simulated by atmospheric general circulation models [*Ginoux and Torres*, 2003; *Yu et al.*, 2003], and

[1]Jet Propulsion Laboratory, California Institute of Technology, Pasadena, California, USA.
[2]NASA Goddard Space Flight Center, Greenbelt, Maryland, USA.

Copyright 2008 by the American Geophysical Union.
0148-0227/08/2008JD010083

Table 1. Satellite Instruments Used for Dust Characterization Studies

Instrument	Full Name	Reference	Products Used
MISR	Multiangle Imaging SpectroRadiometer	*Diner et al.* [2001]	AOT and properties
AIRS	Atmospheric Infrared Sounder	*DeSouza-Machado et al.* [2006]	IR dust mask
MODIS	Moderate Resolution Imaging Spectroradiometer	*Remer et al.* [2005]	AOT, fine/course ratio
CALIOP	Cloud-Aerosol Lidar with Orthogonal Polarization	*Vaughan et al.* [2004]	vertical distribution, AOT
TOMS	Total Ozone Mapping Spectrometer	*Torres et al.* [1998]	aerosol index (AI)
OMI	Ozone Monitoring Instrument	*Torres et al.* [2007]	AI and UV AOT

CALIPSO data were used for identifying and characterizing dust plumes over the Tibetan Plateau [*Huang et al.*, 2007].

[4] A model-simulated climatology by *Jones et al.* [2004] indicates that the westward transport of dust is modulated by African Easterly Waves, which propagate from the west coast of North Africa across the tropical Atlantic. *Gu et al.* [2004] found that the African monsoon consists of two distinct seasons. During the first season, which occurs in late spring and early summer and appears strongly influenced by sea surface temperatures off the coast of West Africa, dust transport is located approximately 5° north of the equator. When the second season arrives in July, the main dust plume moves north, to around 10° north of the equator. On the basis of the Puerto Rico Dust experiment (PRIDE), *Reid et al.* [2002, 2003] suggested the change from the northeast to southwest monsoon along the coast of north Africa during mid July reduces dust particle export in the planetary boundary layer, limiting long-range dust transport to the Saharan Air Layer (SAL). *Tegen and Miller* [1998], *Mahowald et al.* [2003] and *Colarco et al.* [2003] all concluded that the downwind dust distribution is controlled mainly by dynamical transport mechanisms, rather than by the timing of source emissions.

[5] MODIS, aboard the NASA Earth Observing System's Terra satellite, provides aerosol products with approximately 2-day global coverage, whereas instantaneous observations from the companion Multiangle Imaging Spectroradiometer (MISR) instrument capture dust plumes during several stages of their evolution. As the plumes cross the ocean, MISR's multiangle aerosol retrievals complement MODIS's nadir-only observations in sun glint areas, and, through sampling of side scattered light, make it possible to determine aerosol properties and distinguish dust from spherical aerosol components [*Kahn et al.*, 1997, 2001; *Kalashnikova et al.*, 2005; *Kalashnikova and Kahn*, 2006]. MISR's dust retrieval capability over bright deserts, sensitive to total column aerosols [*Martonchik et al.*, 2004], supplements and enhances TOMS and OMI retrievals, which have limited sensitivity to boundary layer aerosols. And MISR standard multiangle stereoheights can be used to determine dust plume physical characteristics near their sources, useful for constraining dust injection heights in aerosol transport models [*Kahn et al.*, 2007a].

[6] In this paper, we analyze in detail four dust events captured by MISR as well as MODIS/Terra, at multiple stages of transatlantic transport during summer 2000: two events during the northeast early summer monsoon season, and two events later in the summer during the southwest monsoon season. For this period, in situ field data were also acquired as part of the Puerto Rico Dust Experiment (PRIDE) field campaign, as well as Aerosol Robotic Network (AERONET) surface-based Sun photometer data at several sites along the dust trajectory. Our goal is to extract the information content of the combined MISR and MODIS aerosol products, for the purpose of quantitatively improving aerosol transport modeling. Specifically, we (1) assess MISR and MODIS AOT and property retrieval quality for transported dust plumes, (2) map AOT evolution that constrains estimates of dust spatial deposition patterns, and (3) study changes in dust properties during transport. The paper is organized as follows: in section 2 we introduce our approach and intercompare MISR and MODIS aerosol products with AERONET data, demonstrating the quality of the latest versions of the MISR and MODIS products in dust-dominated situations. In section 3 we present constraints on dust transport for the four selected cases and analyze retrieved downwind dust properties and deposition patterns. Section 4 summarizes our main results and discusses implications.

2. Satellite Observations and Data Quality Assessment

[7] In this section, we describe briefly the MISR, MODIS, and AERONET data sets used, and make a quantitative assessment of data quality in transported dust situations, by comparing the satellite and surface-based results from these instruments.

2.1. MISR

[8] MISR/Terra is an imaging instrument operating in four spectral bands centered at 446, 558, 672, and 867 nm, at each of nine view angles spread out in the forward and aft directions along the flight path at 70.5°, 60.0°, 45.6°, 26.1°, and nadir. The swath width is about 380 km, spatial sampling is up to 275 m per pixel, absolute radiometric calibration accuracy is about 3%, and global coverage is obtained every 7 to 9 days. MISR's combination of multispectral and multiangle data makes it possible to retrieve some information about particle size, shape, and single-scattering albedo in addition to the aerosol optical thickness (AOT) [*Kahn et al.*, 1998, 2001]. A number of validation studies have shown that MISR provides reliable AOT values (on the order of 0.05 precision), even over bright desert [*Diner et al.*, 2001; *Martonchik et al.*, 2004; *Christopher and Wang*, 2004] A global comparison of AOT for coincident MISR and AERONET data showed that overall, even for an early version of the MISR product, 63% of the MISR-retrieved AOT values in the green band fall within 0.05 or 20% of AERONET AOT, and about 40% are within 0.03 or 10% [*Kahn et al.*, 2005] In addition, *Kahn et al.* [2007a] demonstrated that multiangle stereo height produced by

Table 2. AERONET Validation Sites Used in This Study

Site Name	Latitude	Longitude	Classification	AERONET Data Availability	Number of Counts	
					MISR	MODIS
Saada	31.37°N	−8.89°W	North Africa	Jul 2004 to Jun 2006	79	232
Agoufou	15.28°N	−1.28°W	North Africa	Sep 2003 to May 2007	59	31
Dahkla	23.43°N	−15.56°W	North Africa	Feb 2002 to Oct 2003	55	0
Dakar	14.38°N	−16.95°W	North Africa	May 2000 to Oct 2006	123	487
Cape San Juan	18.23°N	−65.37°W	transported dust	Mar 2005 to May 2007	25	24
La_Parguera	17.58°N	−67.02°W	transported dust	Jul 2000 to Jun 2006	160	680
Guadeloup	16.33°N	−61.51°W	transported dust	Jan 2001 to Jul 2002	30	81
Capo_Verde	16.72°N	−22.93°W	downwind	Jan 2000 to Apr 2007	95	11
Izana	28.18°N	−16.30°W	downwind	Jun 2004 to Oct 2006	98	450

MISR provides plume height estimates in aerosol source regions with uncertainty ±500m.

[9] Particle property validation is a current MISR team effort. On the basis of initial studies, expected MISR sensitivity is 20% to the particle model AOT fraction [*Kahn et al.*, 1998] that translates into the ability to distinguish three to five particle size groupings [*Kahn et al.*, 1998] two to three single-scattering albedo (SSA) types [*Chen et al.*, 2008] and spherical versus nonspherical dust particles [*Kahn et al.*, 1997; *Kalashnikova et al.*, 2005; *Kalashnikova and Kahn*, 2006]. Particle property sensitivity diminishes for midvisible AOT below about 0.15, and over bright surfaces. In this paper, we make use of MISR-derived aerosol particle properties from versions 19–21, the latest available versions of standard level 2 product on the dates of interest, for AOT > 0.2, over ocean.

2.2. MODIS

[10] The MODIS instruments aboard the Terra and Aqua satellites observe Earth in 36 spectral bands from 0.4 to 14.4 microns. Each instrument sees a 2330-km swath, obtaining global coverage in 2 days. Validated MODIS aerosol products include AOT over water and some land, though not over bright desert, and fine-mode fraction [*Remer et al.*, 2005, and references therein]. The AOT uncertainty is ±0.05 (±0.15*AOT) over the land and ±0.03 (±0.05*AOT) over the ocean, and the monthly average fine-mode fraction aerosol optical depth uncertainty is ±20% [*Remer et al.*, 2005] We take advantage of the more frequent MODIS coverage over ocean to complement MISR's AOT results, an especially important synergy for large-scale transport studies. In this study, we use primarily MODIS ocean retrievals from collection 5 of the standard level 2 product.

2.3. AERONET

[11] AERONET [*Holben et al.*, 1998] is a global network of surface-based radiometers, a federation of Cimel Electronique Sun photometers capable of continuous AOT measurements. The AERONET federation includes over 160 stations, and reports daytime aerosol optical thickness on 15-min centers. AERONET aerosol spectral optical thickness is derived from direct beam solar measurements [*Holben et al.*, 2001]. The AERONET product also provides particle property retrievals about once per hour [*Dubovik et al.*, 2000]. The Cimel instruments cover the 340–1600 nm spectral range with typical AOT uncertainties of ±0.015 [*Dubovik et al.*, 2000]. Uncertainties for derived particle microphysical properties vary with conditions; generally, there is higher confidence in particle size constraints than single-scattering albedo [*Dubovik et al.*, 2000]. Currently two AERONET data versions (versions 1 and 2) and three quality levels (levels 1.0, 1.5, 2.0) exist for each product. Although levels 1.0 and 1.5 are provided in near real time, a 12-month or longer delay (due to final calibration and manual inspection) ensures that the highest-quality data can be found in version 2, level 2.0 data products. We use version 2 level 2 AOT data from AERONET stations in the North African/North Atlantic regions (see Table 2) for investigating the quality of MISR and MODIS AOT and Angstrom exponent products. Version 2 level 1.5 AERONET aerosol property data from Capo Verde, Roosevelt Roads and La Parguera AERONET stations, operational during the summer of 2000, are used to study the 2000 dust events, as very little level 2 data are available for this particular season.

2.4. MISR and MODIS Validation Over North Africa and the North Atlantic

[12] As a first step toward using these products, we assessed MISR and MODIS aerosol retrieval quality specifically over the North Africa and the North Atlantic Saharan dust transport regions by comparing with AERONET AOT and Angstrom exponent. We considered all available MISR and MODIS overpasses of the AERONET sites in these areas during 2000–2007, and investigated separately overpasses with data available in MISR 17.6 km or MODIS 10 km retrieval regions that contained AERONET stations (which we call 1 × 1), and overpasses with data averaged over 3 × 3 satellite retrieval regions (which we call 3 × 3). The 3 × 3 averaging increases the amount of data available for satellite-AERONET comparisons, and allows us to compare satellite land and water retrievals near the same AERONET site. Comparison statistics for 1 × 1 and 3 × 3 retrieval regions are also useful for estimating the effects of dust spatial variability at selected sites. Time averaging was performed on AERONET retrievals if more than one measurement was available during a 2-h window bracketing the MISR or MODIS overflights. All AERONET AOT values used for AOT comparison were linearly interpolated to the MISR green band (558 um) wavelength. Cloud contamination limits sampling for both satellite instruments. In particular, few satellite overpasses were coincident with the AERONET sky scan measurements used for property retrievals.

[13] We derived MISR Angstrom exponents as a least squares fit to the MISR-retrieved AOT at the four MISR

wavelengths accounting for the MISR AOT uncertainties. AERONET Angstrom exponent was calculated from the direct sun spectral AOT measurements, with the wavelengths linearly interpolated to the nearest MISR band. The MODIS Angstrom exponents are significantly different from the MISR and AERONET values; therefore, to avoid confusion, and since we do not use the MODIS particle properties in this study anyway, we excluded MODIS Angstrom exponent retrievals from this comparison. We also excluded Angstrom exponent values for overpasses when AERONET midvisible AOT was less that 0.15 because we do not expect satellite sensitivity to aerosol properties at very low optical depths.

[14] We selected 9 AERONET sites located on either side of the North Atlantic, between about 15° and 30°N, that each provide good-quality measurement records at least 2 years long (Table 2). These sites had more than ten coincident MISR-AERONET or MODIS-AERONET AOT matches needed for statistical comparison. Four AERONET sites are located in North Africa (Agoufou, Dahkla, Dakar and Saada), two are ocean sites downwind of North African sources (Izana and Capo Verde), and three are located in the Caribbean, often affected by transported dust (Cape San Juan, Guadeloup and La Parguera). We separately analyze land and ocean satellite retrievals for both MISR and MODIS; very few ocean retrieval matches are available for the 1 × 1 statistics.

[15] Our AOT comparison results for the 3 × 3 averaging are given in Figure 1a for near-source regions and Figure 1b for downwind and dust transport regions (the Cape San Juan site, not shown here, has the least amount of data, but a good regression for both MISR and MODIS AOT). The comparison statistics for both 1 × 1 and 3 × 3 retrieval regions are summarized in Tables 3a and 3b. The MISR-AERONET AOT agreement is good at most AERONET sites, though the satellites tend to overestimate AOT relative to AERONET near the island sites, especially for low AOT conditions (e.g., Izana). The correlation coefficient is ~0.9 for both near-source and downwind regions for direct overpasses (1 × 1 regions), and larger than 0.85 for 3 × 3 averaging. Low optical depth (below 0.05) for more than half the MISR and MODIS overpasses at Izana, combined with assumptions made in the satellite retrieval algorithms about ocean surface optical properties [e.g., *Kahn et al.*, 2007b], contribute to the AOT overestimate there; no high-AOT, dusty days were available for AOT comparisons at this site. There is significantly less AERONET coincident data available for MODIS compared to MISR, despite more extensive MODIS coverage in general. Sun glint contamination over maritime sites and retrieval failures over optically bright desert sites significantly decrease the MODIS data available for these dust-related studies. MODIS-AERONET AOT correlation coefficients at sites where MODIS retrievals are available are generally lower than those for MISR; MODIS land retrievals at Dakar and Agoufou tend to systematically underestimate AOT, whereas at Saada agreement is good, and at the ocean sites of La Parguera, Izana and Guadeloup AOT is systematically overestimated. These results are probably due to different surface property assumptions [e.g., *Kahn et al.*, 2007b], as mentioned above regarding MISR. MODIS collection 5 water retrievals overestimate AOT for all available overpasses at the La Parguera, Izana, and Guadeloup ocean sites. However, overall MODIS-AERONET correlation coefficient at all sites except Agoufou, which has a very bright surface, and the very low AERONET AOT conditions at Izana, are larger that 0.75 and therefore acceptable for dust transport studies.

[16] Comparisons of MISR Angstrom exponents with those derived from AERONET AOTs are shown on Figure 2. In some cases MISR tends to systematically underestimate (Saada) and in a few cases overestimate (Dakar) Angstrom exponent compared to AERONET. These errors are most likely due to the limited range of particle sizes and mixtures available in the standard aerosol retrieval algorithms, and are the subject of ongoing studies by the MISR team. However, on the basis of Figure 2, the retrieval accuracy is sufficient to distinguish predominantly large from predominantly medium-sized particles, and the majority of retrieved values for these cases correspond to AERONET Angstrom exponent less than 1, as expected for large dust and sea salt particles. Exclusion of Angstrom exponent values corresponding green-band AOT less than 0.5 (not shown) improves the comparison but significantly reduces amount of data available for the analysis. The MISR Angstrom exponent is not yet validated; changes in the Standard algorithm spherical components [e.g., *Chen et al.*, 2008], and possible refinement of the coarse mode dust optical model [*Kalashnikova et al.*, 2005], are likely to improve MISR Standard retrieval particle property results. Currently available MISR Angstrom exponent, taken together with MISR spherical AOT fraction, makes it possible to separate thick dust plumes (AOT > 0.5) from other aerosol air mass types.

[17] No data points are available for MISR-MODIS AOT intercomparison over the Atlantic, because, as we demonstrate in the next section, MISR and MODIS retrievals are always spatially complementary over the tropical ocean for these events.

[18] In summary, our correlation statistics demonstrate that the latest MISR and MODIS AOT data quality is sufficient for the dust transport studies and transport model validation.

3. Saharan Dust Plume Evolution During Transoceanic Transport

[19] In this section we characterize the AOT and particle property evolution of Saharan dust outbreaks during transoceanic transport, using the MISR and MODIS aerosol products.

3.1. Deposition Patterns From MISR and MODIS AOT Observations

[20] We used the MODIS collection 5 level 3 daily averaged aerosol product and NRL Aerosol Analysis and Prediction System (NAAPS) model predictions to select dust events for our study. The NAAPS model [*Christensen*, 1997; *Westphal et al.*, 1988] uses global meteorological analyses and forecasts from the Navy Operational Global Atmospheric Prediction System (NOGAPS) [*Hogan and Rosmond*, 1991; *Hogan and Brody*, 1993] on a 1 × 1° grid, at 6-h intervals and 18 vertical levels reaching 10 km. NAAPS has been operating since 1998 and is updated

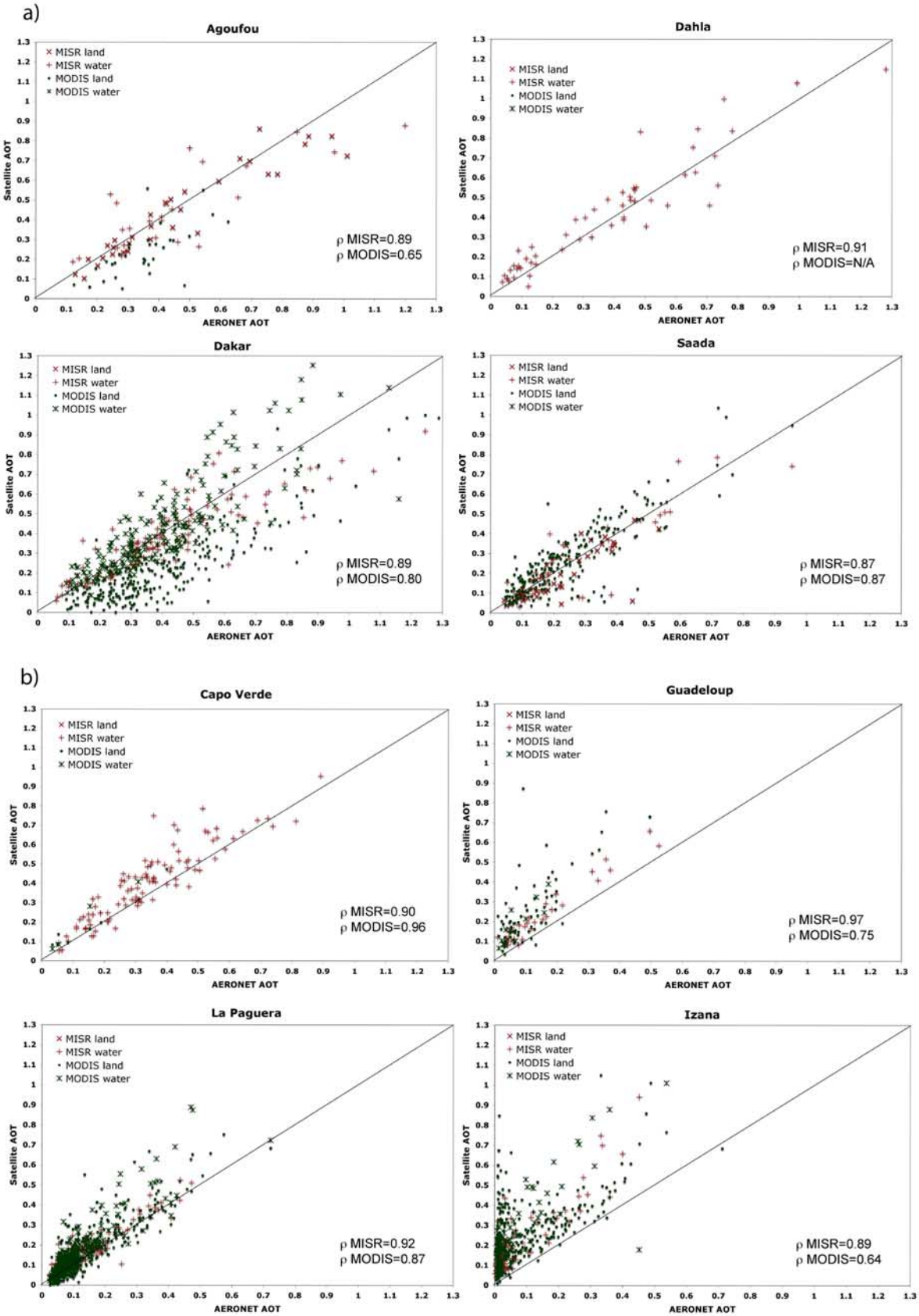

Figure 1. MISR-MODIS-AERONET AOT and Angstrom exponent comparisons at dusty AERONET sites. (a) Agoufou, Dahkla, Dakar, and Saada (near sources) and (b) Capo Verde, Izana (downwind), La Parguera, and Guadeloup (Caribbean). ρ is the correlation coefficient.

Table 3a. AERONET-MISR Comparison Statistics at AERONET Validation Sites

AERONET Site	MISR Mean AOT		AERONET Mean AOT		Mean AOT Difference[a] (%)		Correlation Coefficient		Regression Slope		Regression *Y* Intercept	
	1 × 1	3 × 3	1 × 1	3 × 3[b]	1 × 1	3 × 3	1 × 1	3 × 3	1 × 1	3 × 3	1 × 1	3 × 3
Agoufou	0.34	0.39	0.34	0.40	9.51	9.67	0.93	0.89	0.98	0.77	0.02	0.09
Saada	0.14	0.17	0.19	0.37	22.4	16.5	0.89	0.87	0.98	0.88	-0.02	0.01
Izana	0.10	0.16	0.03	0.03	105	371	0.39	0.89	0.27	1.43	0.10	0.10
CapoVerde	0.31	0.36	0.28	0.30	10.2	15.3	0.93	0.90	0.94	0.98	0.04	0.07
Dahkla	0.31	0.33	0.26	0.28	18.8	17.6	0.91	0.91	0.90	0.79	0.06	0.08
Dakar	0.33	0.34	0.34	0.36	12.5	12.8	0.91	0.89	0.72	0.68	0.09	0.10
CapeSanJuan	0.14	0.13	0.11	0.09	25.7	30.0	0.99	0.86	1.11	0.85	0.02	0.05
Guadeloup	N/A	0.20	N/A	0.11	N/A	67.2	N/A	0.97	N/A	1.10	N/A	0.06
La_Parguera	0.11	0.13	0.09	0.10	18.2	24.6	0.92	0.92	0.96	0.96	0.03	0.03

[a]The mean AOT difference is the average value of ABS ((MISR-AERONET)/AERONET), expressed as a percent, where MISR and AERONET are AOT evaluated in each MISR spectral band. Few events, for which the AERONET AOT is extremely low, are responsible for the high mean AOT difference values in some cases [see *Kahn et al.*, 2005].

[b]These are AERONET values aggregated over all days for which there were retrievals within any of the 3 × 3 MISR retrieval regions surrounding the AERONET site; there are many more events for the 3 × 3 than the 1 × 1 means in most cases.

every 6 h as each NOGAPS analysis becomes available. Every 12 h, a 5-day forecast is carried out. The global simulations of sulfate, dust, and smoke AOT for various regions of the world are posted daily at http://www.nrlmry.navy.mil/aerosol along with daily satellite aerosol analyses for comparison purposes.

[21] We investigated the region from 0° to 25°N latitude and from 15° to 75°W longitude during summer 2000. The NAAPS model predicts almost continuous dust activity over North Africa (lat. 0 to 25°N) in June and several back-to-back dust outbreaks in July. Dust events over North Africa in June and July 2000 lasted for several days and often overlapped, making it difficult to identify and track individual plumes. However, a few major dust clouds met all these conditions: (1) they were predicted by NAAPS, (2) they were observed by the combination of MODIS/MISR and the AERONET stations at Cape Verde and Puerto Rico, (3) they crossed the northwest coast of Africa, and (4) they were identified in the satellite data well into the Atlantic.

[22] NAAPS and MODIS Hovmoller diagrams illustrate June–July dust event extent and duration (Figure 3). On the basis of the NAAPS modeled AOT dust fraction over the Atlantic and the MODIS daily averaged AOT, we identified four cases of transported dust when MISR obtained good coverage of the cloud on 3 or more days during transit. These events are summarized in Table 4 as cases 1 through 4.

[23] MISR and MODIS-Terra AOT retrievals are complementary over the transported dust region, and since MISR coverage is not limited by sun glint, it adds significantly to the overall AOT picture. Figure 4a gives an example of MISR plume tracking for case 2, beginning on day 1, with the plume off the coast of Africa, through day 5, when it reached Puerto Rico. For this event, the MISR swath misses the plume after day 3 of transport. However, the addition of MODIS data (Figure 4b) shows the plume located east of Puerto Rico on day 5 (8 July), and actually reaching Puerto Rico on day 6 (9 July). For Figure 4, the AOT = 0.15 and AOT = 0.5 contours are superposed on the image, as yellow and purple lines respectively, to highlight plume extent.

[24] Figure 5 summarizes the satellite coverage for case 1 (Figure 5a), during early summer and cases 3 (Figure 5b) and 4 (Figure 5c), during late summer. The midvisible AOT = 0.15 and AOT = 0.5 contours have been superposed on Figure 5 as well, to highlight plume evolution. For all cases, the MISR swaths are fully contained within the MODIS sun glint regions, where MODIS AOT retrievals were not performed, filling in key areas that would otherwise be missing. Also note that for case 2, MISR did not observe the plume on day 3, because of a data acquisition failure early in the Terra mission.

[25] To more fully document dust transport and deposition patterns quantitatively from the combination of MISR and MODIS data, we also analyzed how dust plume surface area evolved over the Atlantic. For convenience, we define the "total plume surface area" as the area within the MISR and/or MODIS field of view having midvisible AOT > 0.15.

Table 3b. AERONET-MODIS Comparison Statistics at AERONET Validation Sites

AERONET Site	MODIS Mean AOT		AERONET Mean AOT		Mean AOT Difference[a] (%)		Correlation Coefficient		Regression Slope		Regression *Y* Intercept	
	1 × 1	3 × 3	1 × 1	3 × 3	1 × 1	3 × 3	1 × 1	3 × 3	1 × 1	3 × 3	1 × 1	3 × 3
Agoufou	0.27	0.20	0.36	0.33	22.4	29.5	0.76	0.65	0.70	0.72	0.02	−0.01
Saada	0.25	0.21	0.22	0.19	19.4	23.2	0.91	0.87	0.99	1.01	0.03	0.02
Izana	0.22	0.20	0.01	0.01	327	377	0.61	0.64	0.78	0.98	0.24	0.18
CapoVerde	N/A	0.16	N/A	0.10	N/A	29.9	N/A	0.96	N/A	1.07	N/A	0.04
Dahkla	N/A	N/A	N/A	N/A	N/A	N/A	N/A	N/A	N/A	N/A	N/A	N/A
Dakar	0.20	0.24	0.36	0.36	37.3	25.8	0.95	0.80	0.86	0.85	−0.08	−0.02
CapeSanJuan	N/A	0.11	N/A	0.13	N/A	22.6	N/A	0.85	N/A	0.86	N/A	0.01
Guadeloup	0.19	0.20	0.12	0.08	81.2	1.24	0.59	0.75	1.28	1.43	0.07	0.09
La_Parguera	0.10	0.01	0.09	0.01	24.3	0.1	0.83	0.87	1.09	1.14	0.02	0.01

[a]The mean AOT difference is the average value of ABS ((MODIS-AERONET)/AERONET), expressed as a percent, where MODIS and AERONET are AOT evaluated in each MODIS spectral band. Few events, for which the AERONET AOT is extremely low, are responsible for the high mean AOT difference values in some cases [see *Kahn et al.*, 2005].

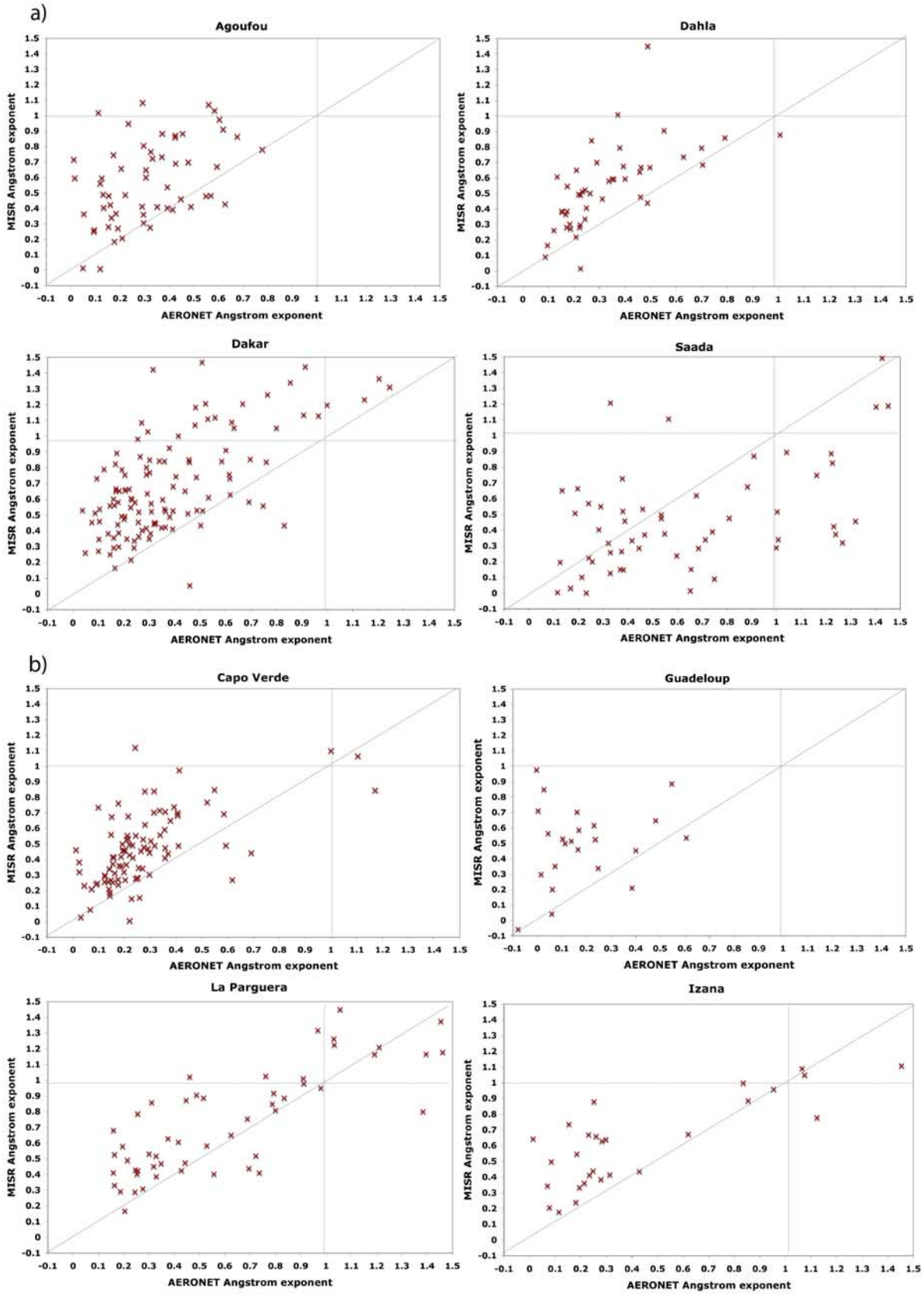

Figure 2. MISR-AERONET Angstrom exponent comparisons at dusty AERONET sites. (a) Agoufou, Dahkla, Dakar, and Saada (near sources) and (b) Capo Verde, Izana (downwind), La Parguera, and Guadeloup (Caribbean).

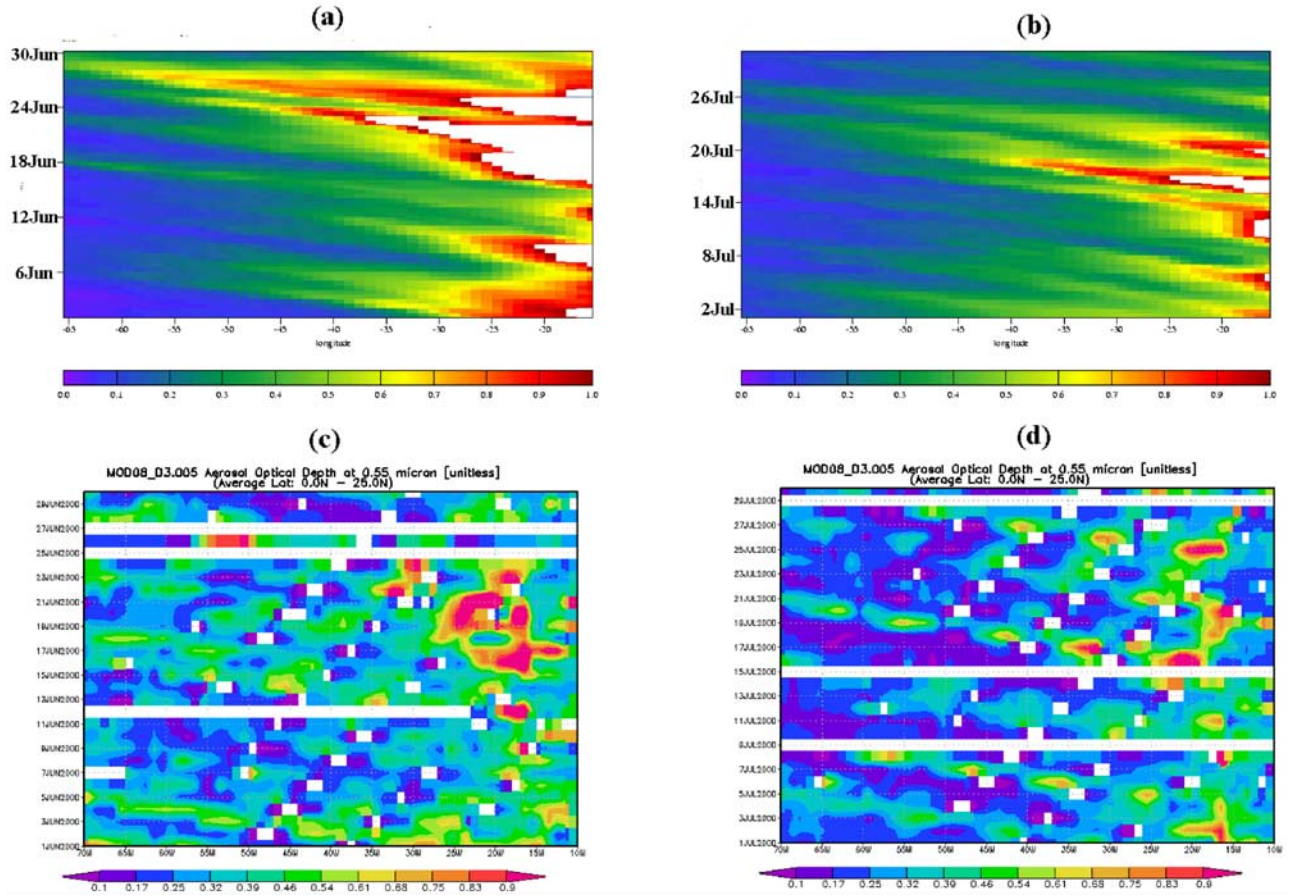

Figure 3. Hovmoller diagrams (longitude versus time AOT plots), average over 0°N to 25°N latitude range. (a) June 2000 NAAPS, (b) July 2000 NAAPS, (c) June level 3 MODIS, and (d) July 2000 level 3 MODIS. Features extending toward the top left in these diagrams are propagating westward.

Taking case 1, for example, MODIS AOT coverage provides between 45 and 56% of the observed total plume area, and MISR contributes the other half (Figure 6). MISR and MODIS AOT retrievals are reasonably consistent across the dust plume, as demonstrated in Figure 7 for the 18 June (downwind of sources) and 22 June (transported plume) examples. MISR-retrieved AOT are always within the range of retrieved MODIS values for all cases selected. Complete, quantitative analysis of plume area evolution is sometimes difficult, as the plume might not be completely imaged even in combined satellite observations. However, the AOT contours in Figures 4 and 5 provide systematic constraints that can be compared with aerosol transport model simulations.

[26] In all cases, the average AOT of the plume from combined MISR and MODIS observations decreases gradually as the plume is transported across the Atlantic, as might be expected (Figure 8). Some patterns emerge, even qualitatively. For example, despite higher AOT on day 1, the case 1 plume reached Puerto Rico on day 6 of transport. For case 5, it took just 5 days for the plume to reach Puerto Rico. More generally, for the early summer cases 1–2, transport took 6 days, whereas the late summer case 3–4 plumes made the journey in about 5 days. In addition, for the two early summer cases, the plumes extended mostly in the northwest direction, whereas the case 4 and 5 plumes extended mostly southwest. Observed variations might be due to the local atmospheric conditions; additional cases

Table 4. Summary of MISR Coverage for Four Major Saharan Dust Transport Events During Summer 2000

Name	Event	Day 1	Day 2	Day 3	Day 4	Day 5	Day 6
Case 1	18–23 Jun	18 Jun: orbit 2667, path 210	19 Jun: orbit 2682, path 217	20 Jun: orbit 2697, path 224	21 Jun: orbit 2712, path 231	22 Jun: orbit 2727, path 5	23 Jun: orbit 2742, path 12
Case 2	4–9 Jul	4 Jul: orbit 2900, path 210	5 Jul: orbit 2915, path 217	6 Jul: orbit 2930, path 224	no MISR data	8 Jul: orbit 2960, path 5	9 Jul: orbit 2975, path 12
Case 3	20–25 Jul	20 Jul: orbit 3133, path 210	21 Jul: orbit 3148, path 217	22 Jul: orbit 3163, path 224	23 Jul: orbit 3178, path 231	24 Jul: orbit 3193, path 5	25 Jul: orbit 3208, path 12
Case 4	22–27 Jul	22 Jul: orbit 3162, path 208	23 Jul: orbit 3177, path 215	24 Jul: orbit 3192, path 222	25 Jul: orbit 3207, path 229	26 Jul: orbit 3222, path 3	27 Jul: orbit 3237, path 10

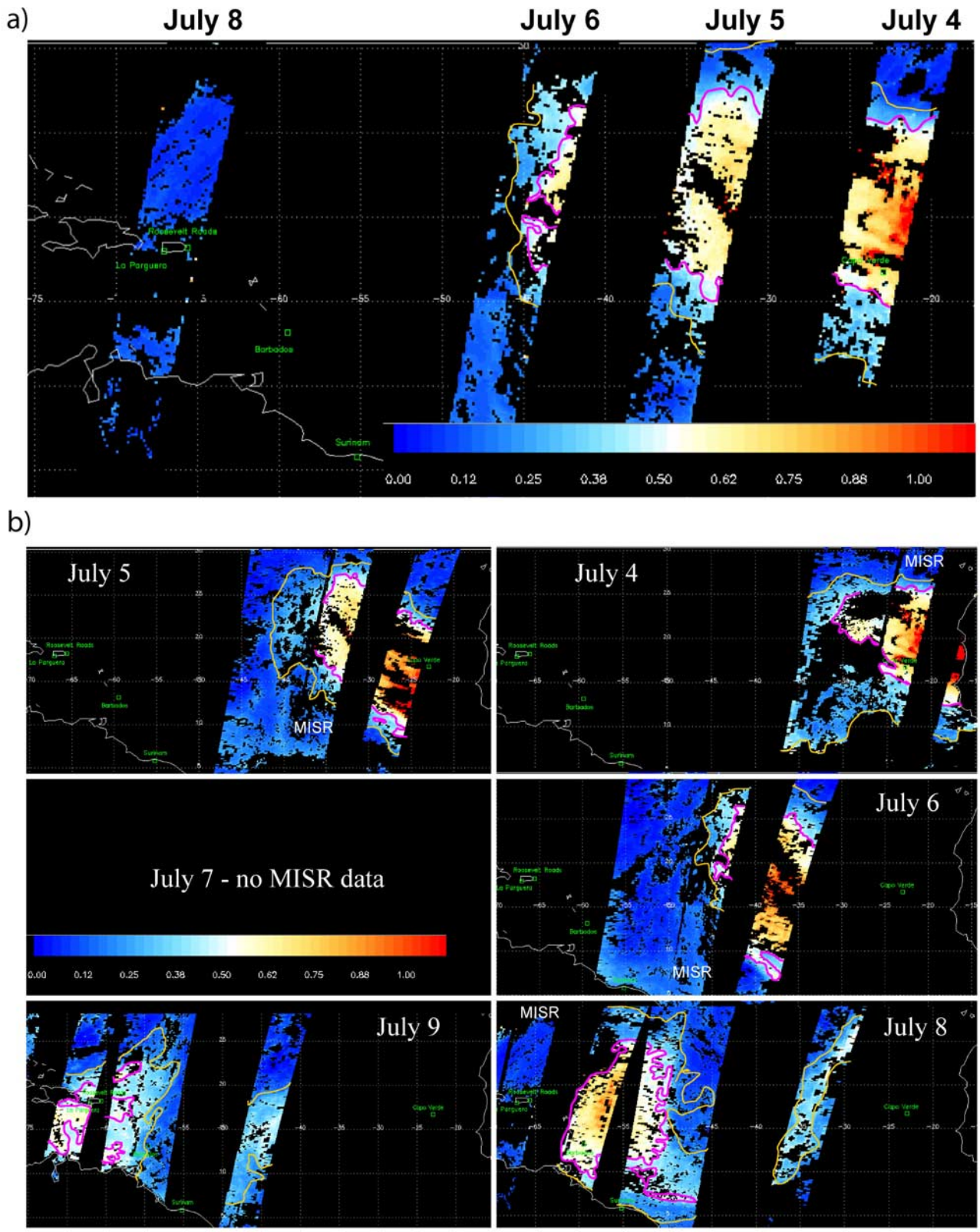

Figure 4. Example of dust plume tracking for case 2. (a) MISR observations, aggregated over the entire period of transit, and (b) complementary MISR and MODIS coverage on days 1–6, 4–9 July. The midvisible AOT = 0.15 and AOT = 0.5 contours have been superposed as very thin, bright yellow and purple lines, to highlight plume evolution.

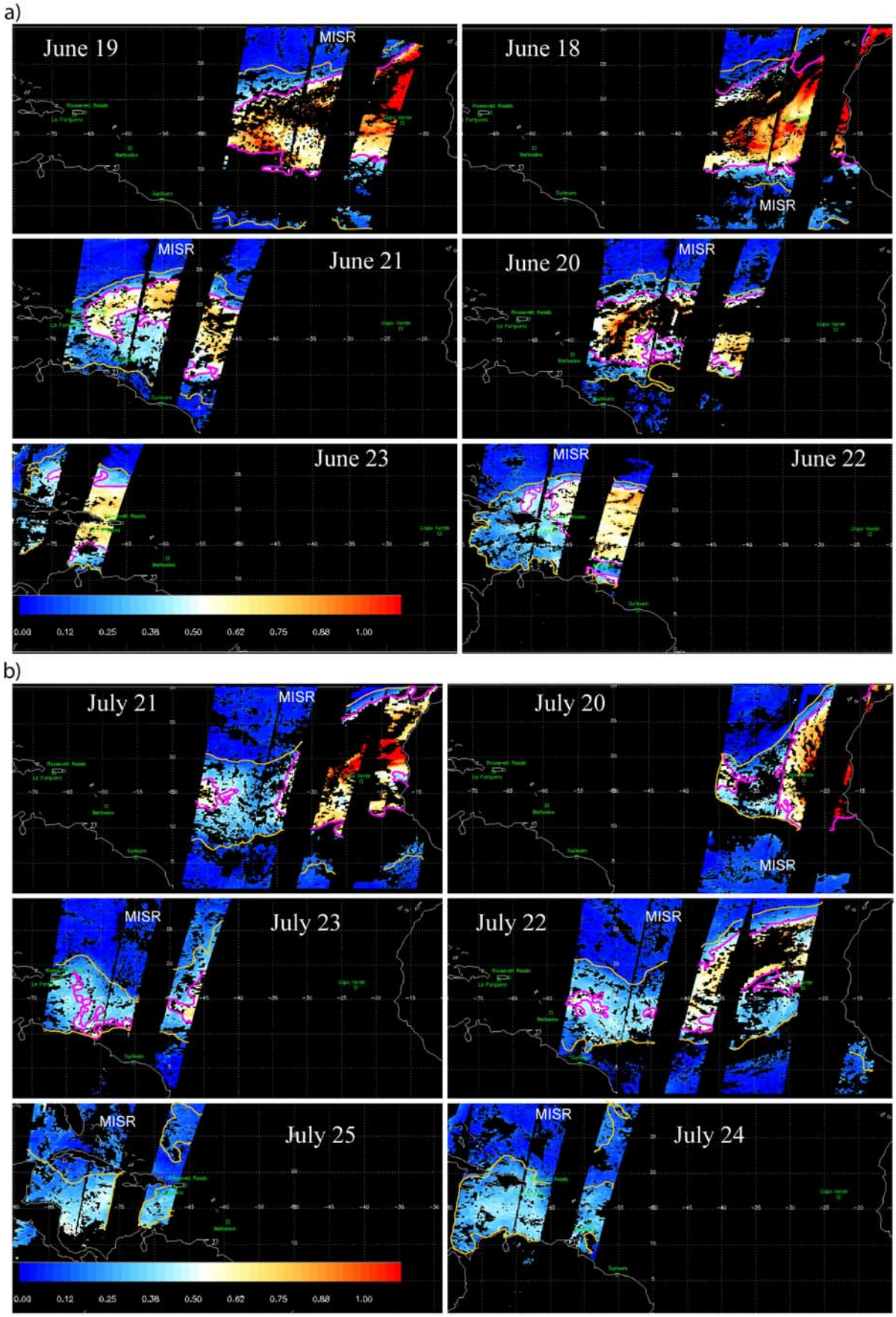
a)
June 19
MISR
June 18
MISR
MISR
June 21
June 20
MISR
June 23
MISR
June 22
0.00 0.12 0.25 0.38 0.50 0.62 0.75 0.88 1.00
b)
July 21
MISR
July 20
MISR
MISR
July 23
July 22
MISR
MISR
July 25
MISR
July 24
0.00 0.12 0.25 0.38 0.50 0.62 0.75 0.88 1.00

Figure 5

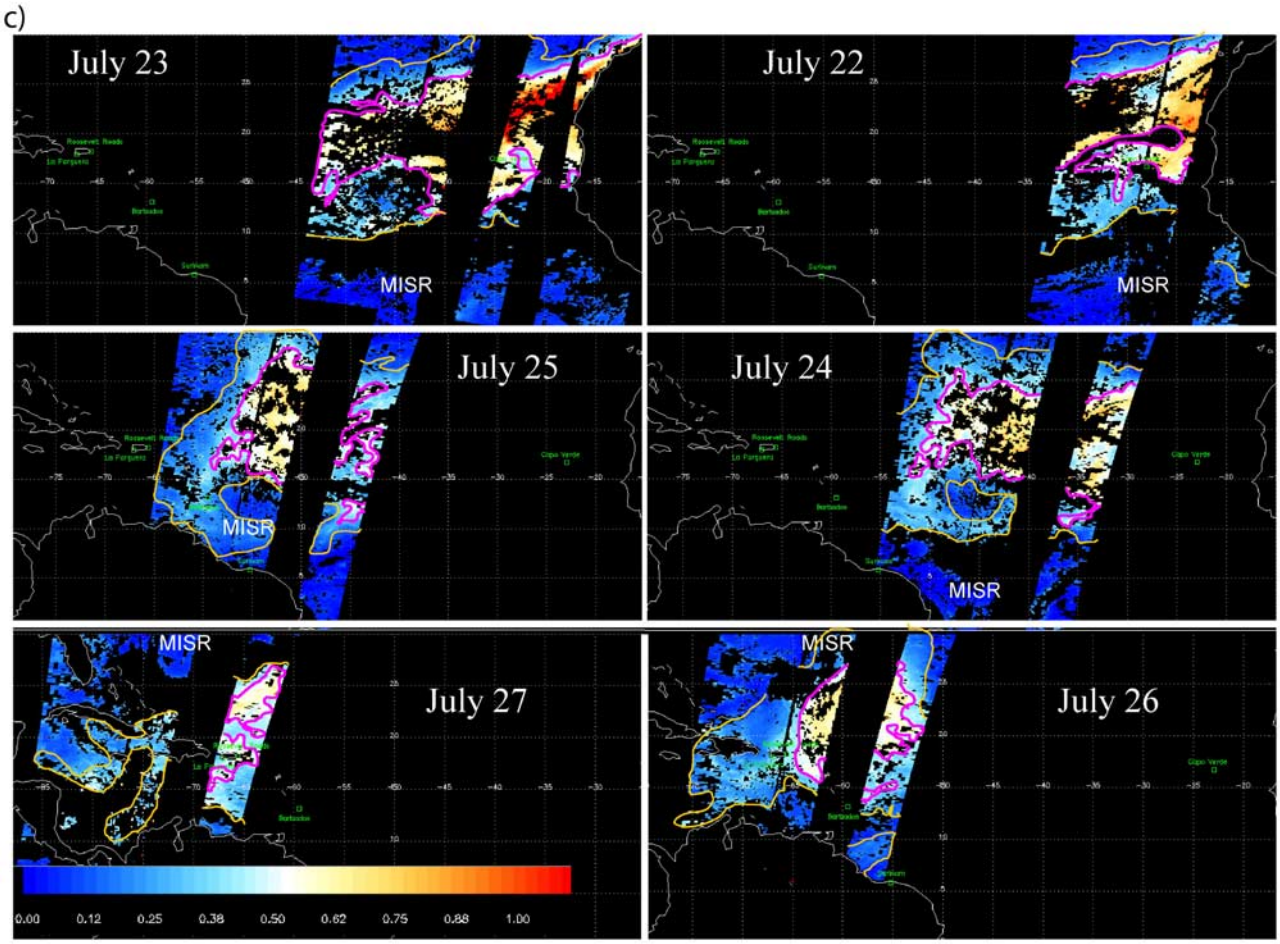

Figure 5. (continued)

combined with transport model analysis are needed to better assess these observations, and will be performed in follow-up work.

3.2. Dust Property Evolution

[27] Because of the lack of coincident data, we were not able to directly compare MISR and AERONET AOT and retrieved properties on both sides of the Atlantic in the presence of dust for the same transport event. In case 1, MISR had good coverage of the Puerto Rico AERONET site during the dusty day but AERONET was not operating. In cases 2 and 4, MISR and AERONET both had data at Puerto Rico but the dust plume dissipated over the ocean or was transported north of Puerto Rico as it crossed the ocean. For the remaining case, MISR also observed dust cloud evolution, but did not have coverage over the AERONET sites at the critical times. However, taken together, the available data provide a picture of dust cloud evolution that we can use both to estimate dust transport and to critically test transport model performance.

[28] AERONET stations on both sides of the Atlantic observed three of the four events. Table 5 summarizes available AERONET level 1.5 data at Capo Verde and the Puerto Rico La Parguera and Roosevelt Roads stations. Overall, AERONET data show that AOT decreases, Angstrom exponent increases and the median radius of a lognormal size distribution fit decreases slightly (~15%) across the ocean. All these trends are as expected if the plume is losing large dust particles during transport. Retrieved values of SSA are similar on both sides of Atlantic and vary between 0.95 and 0.98, characteristic of weakly absorbing dust mixed with mostly nonabsorbing, background spherical particles.

[29] To provide further context, Figure 9 summarizes AERONET-retrieved properties for all available June–July 2000 days with AOT > 0.5 upwind at Capo Verde (Figure 9a) and AOT > 0.3 downwind at Roosevelt Roads (Figure 9b). During the summer season, increased AOT normally corresponds to dust events. Figure 9 demonstrates that Angstrom exponent and particle size are correlated with

Figure 5. Dust plumes tracked across the Atlantic Ocean with combined MISR and MODIS AOT observations. (a) Case 1, 18–23 June; (b) case 3, 20–25 July; and (c) case 4, 22–27 July. The midvisible AOT = 0.15 and AOT = 0.5 contours have been superposed as very thin, bright yellow and purple lines, to highlight plume evolution.

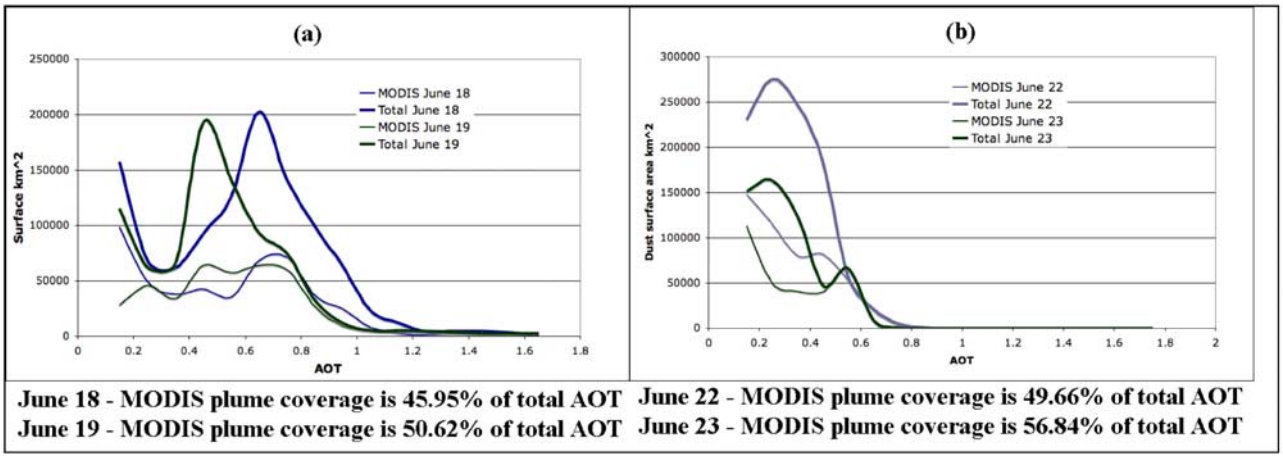

Figure 6. Dust plume area as a function of midvisible column AOT for (a) the first 2 and (b) the last 2 days of case 1 (18–23 June), based on MODIS only and MODIS+MISR retrieved values. The AOT = 0.15 contour is used to define plume area.

AOT, and correspondingly decrease and increase with an increase of AOT values, as expected if the primary variable is dust AOT fraction.

[30] Figure 10 demonstrates MISR's ability to retrieve dust properties in addition to AOT. In this example MISR tracks plume properties for case 1, beginning on day 1, with the plume off the coast of Africa, through day 5, when it reached Puerto Rico. All properties shown are for AOT > 0.15, as MISR property sensitivity diminishes for very low optical depths. As expected, MISR retrieves low Angstrom exponent values, and high nonspherical AOT Fraction values over the thicker parts of the plume; single-scattering albedo values are large (~0.98) over thick plume areas, also as expected. Note that nonspherical particles are sometimes reported in low AOT regions outside the plume (Figure 10c). Under these conditions, the MISR aerosol algorithm might be picking up subvisible cirrus; there are also viewing geometry limitations at low latitudes in some seasons that reduce sensitivity to particle shape. These issues are the subject of studies beyond the scope of the current paper.

[31] We investigated MISR-retrieved aerosol properties averaged first for AOT > 0.15 (the "total" plume), which is also the approximate MISR property retrieval sensitivity limit, and then over the optically thicker areas (AOT > 0.5). Figure 11 summarizes our analysis. Nonmonotonic behavior of MISR-retrieved properties is most likely due to gaps in satellite coverage, since the same parts of the plume were not imaged on all days. MISR-retrieved Angstrom exponent and AOT spherical fraction are ~30% lower in the optically thicker parts of the plume compared to the total plume; that is, Angstrom exponent and sphericity decrease as AOT increases. Within the limits of MISR property retrieval uncertainty, Angstrom exponent and AOT nonspherical fraction, averaged over the total plume (AOT > 0.15), are similar during all stages of transport. However, for the thicker part of the plume (AOT > 0.5), where we expect greater property retrieval sensitivity, the average Angstrom exponent increases about 30% (from ~0.25 to ~0.35), and AOT nonspherical fraction decreases over 50% (from ~0.7–0.8 to ~0.4–0.5), between day 1 and day 6 of

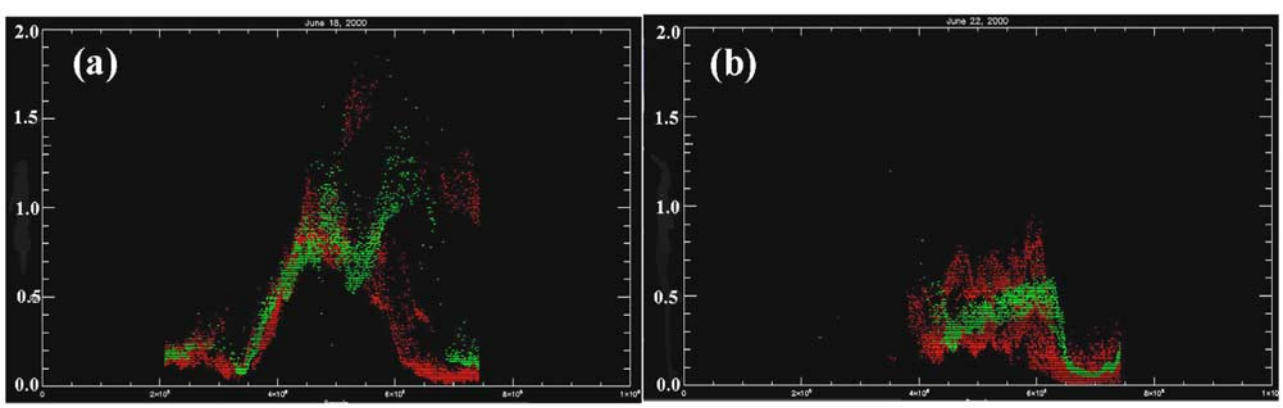

Figure 7. Correspondence of dust plume AOT at the boundary between MISR and MODIS coverage. MISR (green) and MODIS (red) AOT pixels (x axis) versus retrieved AOT values where coverage is contiguous. (a) Dust plume over the Capo Verde, 18 June 2000, and (b) transported dust plume over the Atlantic, 22 June 2000.

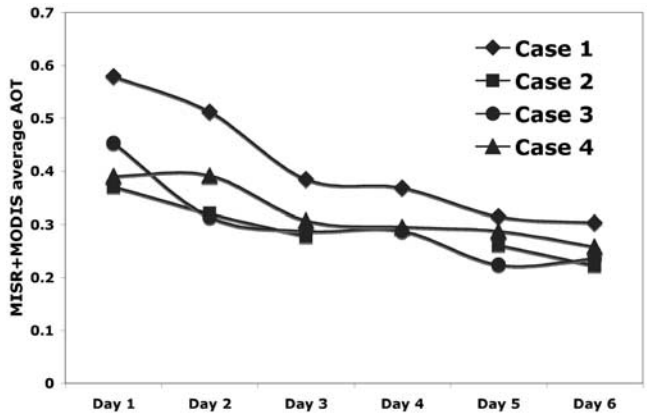

Figure 8. AOT evolution as observed by MISR and MODIS for four cases, during 6 days of transatlantic transport. Day 1 corresponds to the day the plume crosses the west African coast. The quantity shown is AOT averaged over the plume area for which AOT > 0.15.

transport. Such changes would be expected as dust is mixed externally with other aerosol components, and is possibly lost, during transit. In addition to the quantitative result, Figure 11 demonstrates more generally that MISR is sufficiently sensitive to Angstrom exponent and AOT nonspherical fraction to map the evolution of these optical properties during dust transport. Variations in transported dust SSA are below MISR sensitivities; MISR retrieves an average SSA of ~0.98, representative of weakly absorbing dust and background maritime particles.

[32] In addition to AOT and particle property retrievals, dust plume heights can be derived from MISR hyperstereo observations, in places where plume features are discernable in multiple angular views, conditions that are most frequently met near aerosol sources [e.g., *Kahn et al.*, 2007a, Figure 13]. Beyond the MISR Standard Stereo Height product, a new tool called the MISR Interactive explorer (MINX) makes it possible to retrieve height and along track/cross track wind components simultaneously, for individual plumes (http://www-misr2.jpl.nasa.gov/EPA-Plumes/). Although the dust was too uniform and optically thin for MISR stereo height retrievals in most of our transported dust cases, we obtained meaningful plume height retrievals over the water near Capo Verde on 18 June 2000 (Figure 12). In this case, green band AOT, averaged over the plume area outlined in Figure 10, is 0.72. As expected for transported dust, the dust layer was located between 3 and 4 km above the geoid, and realistic wind corrections adjusted plume heights from ~3.2 to 3.7 km. A more extensive study of dust plume height, near-source primarily with MISR as well as downwind using the space-based CALIPSO lidar is possible, but is beyond the scope of the current paper.

4. Conclusions

[33] This paper explores the potential of combining MISR and MODIS-Terra satellite aerosol products and AERONET ground-based observations for improving dust aerosol representations in climate and forecast models. With four cases of transatlantic dust transport during summer 2000, we demonstrate MISR and MODIS capabilities to quantitatively map (1) plume extent over water, (2) AOT evolution for each event, and (3) effective particle size and fraction spherical evolution for thick parts of the plume. We validate these capabilities using AERONET data, and show how MISR complements MODIS in terms of coverage over water. Extensive comparison of MISR and MODIS AOT retrievals with AERONET observations in dusty regions shows accuracies of about 20%; MISR Angstrom exponent is predominantly less than one, in reasonable agreement with AERONET.

[34] For four selected events, we find that, as dust is transported across the Atlantic, AOT and fraction AOT nonspherical systematically decrease, whereas Angstrom exponent increases, as would be expected if dust is progressively diluted with background maritime particles and/or lost from the atmosphere. Within MISR retrieval uncertainties, Angstrom exponent and AOT fraction spherical are lower in the optically thicker parts of the plume by up to 30%, and increase as the plume is transported across the ocean also by about 30% for the thicker part of the plume (AOT > 0.5), where we expect greater property retrieval sensitivity. AOT nonspherical fraction decreases over 50% (from ~0.7–0.8 to ~0.4–0.5) for the thicker part of the plume, between day 1 and day 6 of transport. Retrieved single-scattering albedo (SSA) values are ~0.98 for all stages of plume evolution. For the cases studied, AERONET shows similar property patterns at points on either side of the Atlantic. In our study, the early season cases make the transoceanic journey in 5 days, whereas the later season

Table 5. AERONET Version 2, Level 1.5 Property Retrievals for Selected Events Downwind of Dust Sources (Capo Verde Station) and at Puerto Rico (La Parguera Station)

	Case 2		Case 4	
	4 July, Capo Verde	9 July, La Parguera	21 July, Capo Verde	24 July, La Parguera
AOT 440	0.647	0.319	0.566	0.355
AOT 670	0.622	0.293	0.523	0.328
SSA_{670}	0.954	0.961	0.988	0.937
Angstrom	0.130	0.240	0.189	0.222
R_{eff_course}	1.983	1.636	1.743	1.670
R_{vol_median}	2.424	2.018	2.003	1.893

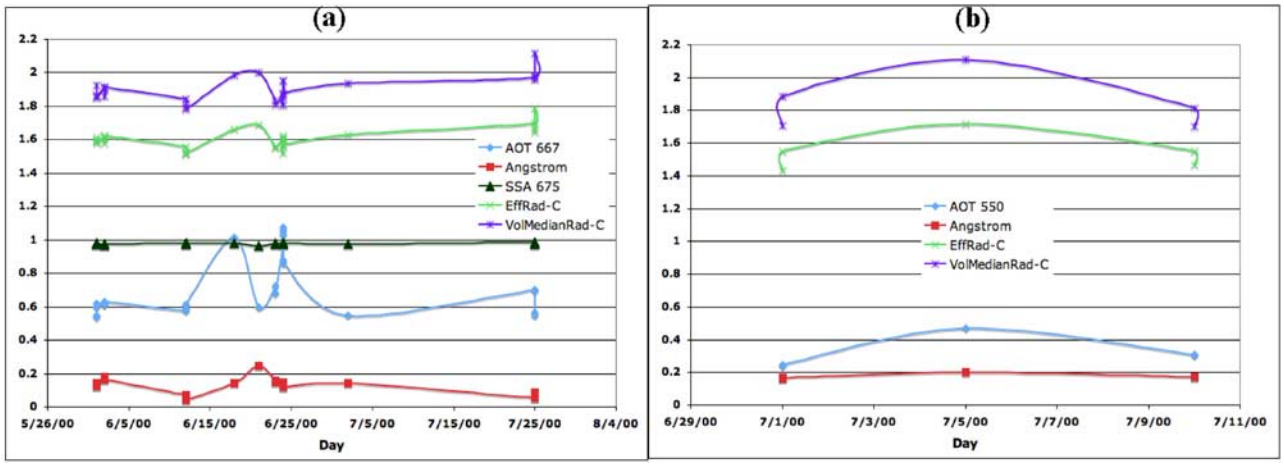

Figure 9. AERONET level 1.5 property retrievals during dusty days. (a) At Capo Verde, just downwind of the source region, for AOT > 0.5, and (b) at Roosevelt Roads, Puerto Rico (transported dust), for AOT > 0.3.

cases take 6 days, though our sample is too small for this conclusion to be more than suggestive.

[35] The results presented here can be used to constrain quantitatively aerosol transport model removal rate and horizontal transport calculations. Combined MISR and MODIS observations map systematic changes in retrieved plume surface area, on the basis of AOT contours; these reflect differences in aerosol dispersion and removal rates that must be reproduced by models. A model constrained in this way can then be used to calculate dust flux, dust deposition, and dust radiative effect with greater accuracy than before. Further improvements in predicting dust impact

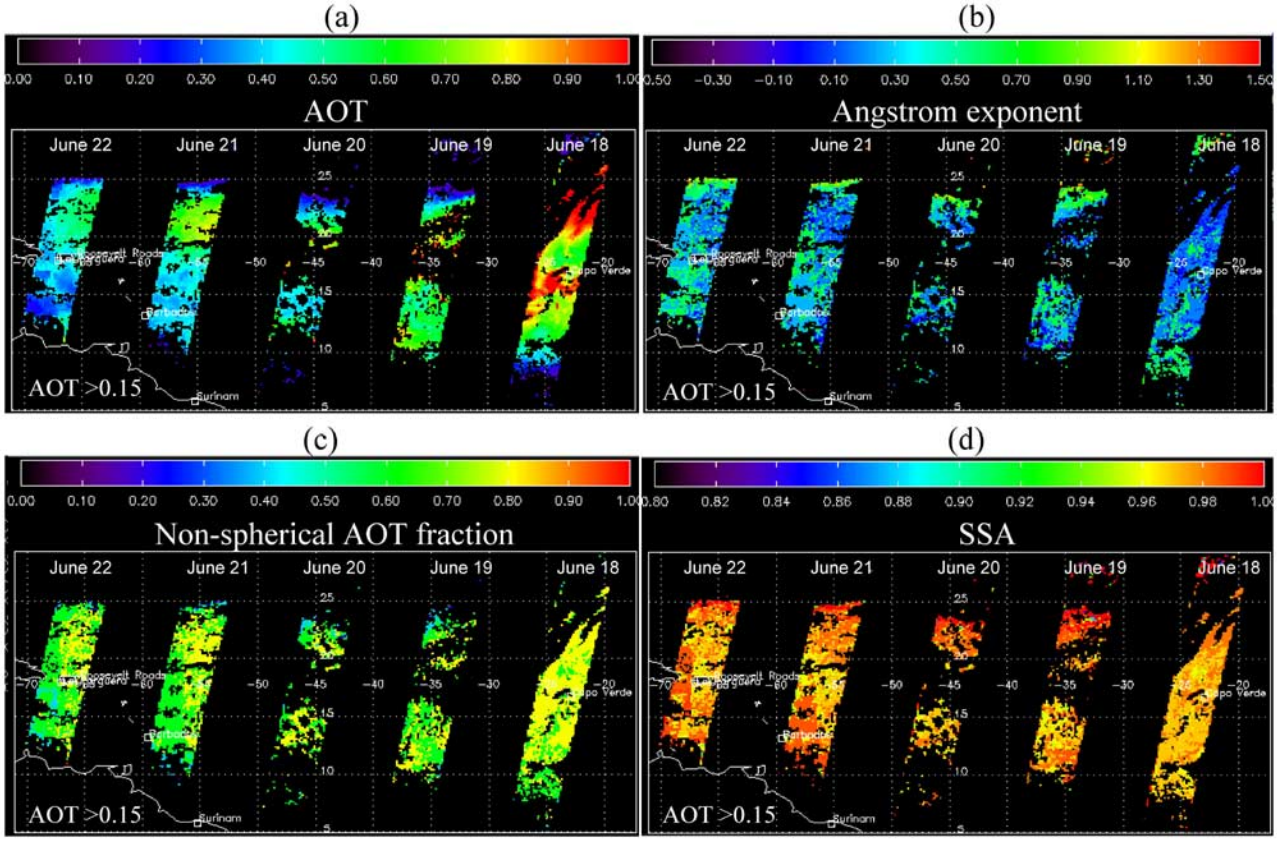

Figure 10. Example of dust plume property evolution, showing MISR-retrieved aerosol property maps, aggregated over the 5-day transit from the African coast to Puerto Rico for case 1. (a) AOT, (b) Angstrom exponent, (c) nonspherical AOT fraction, and (d) SSA.

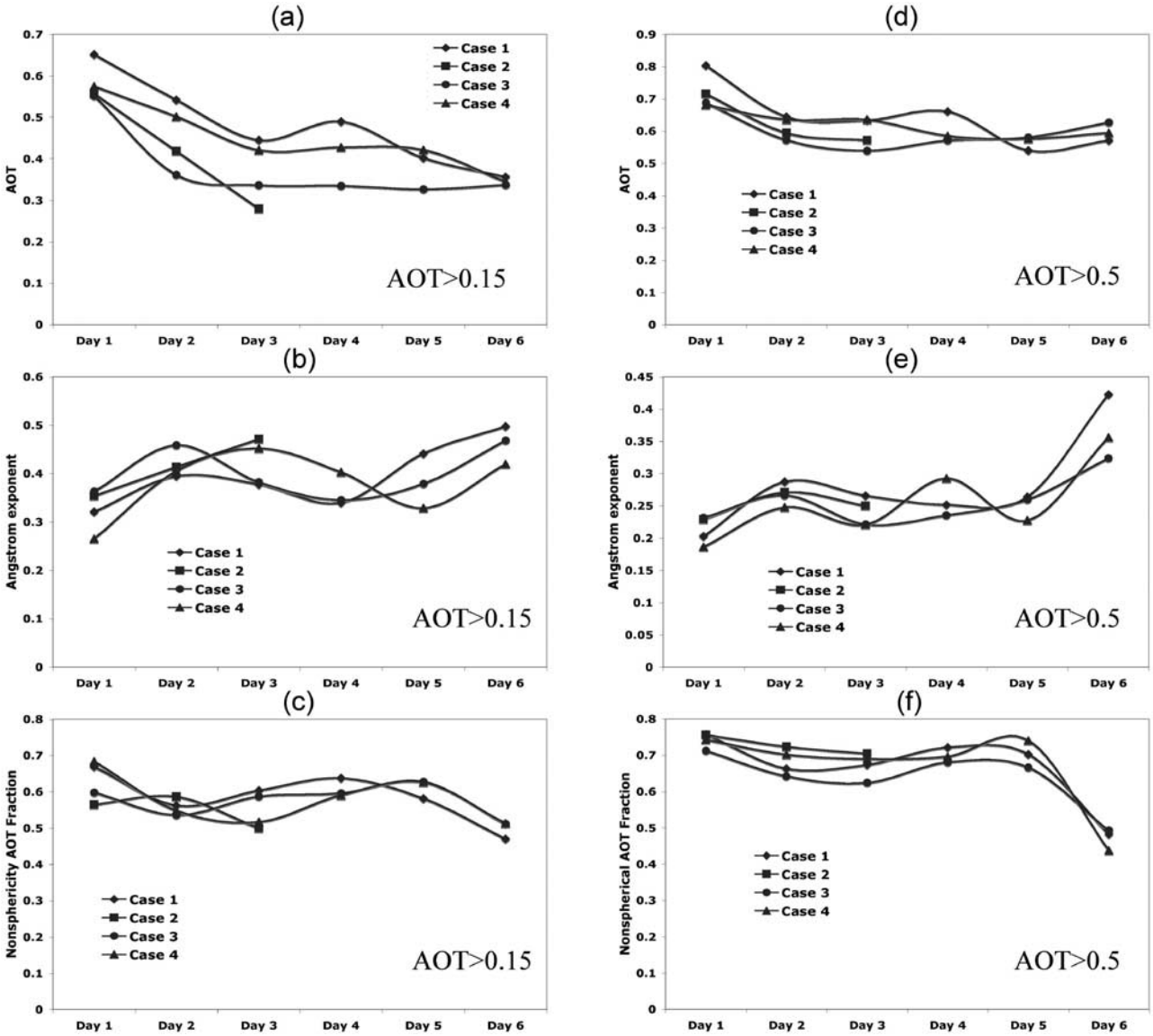

Figure 11. AOT, Angstrom exponent and AOT nonspherical fraction evolution retrieved by MISR for different stages of dust transport. Averaged over the plume area covering AOT > 0.15: (a) AOT, (b) Angstrom exponent, and (c) AOT nonspherical fraction. Averaged over the plume area covering AOT > 0.5: (d) AOT, (e) Angstrom exponent, and (f) AOT nonspherical fraction.

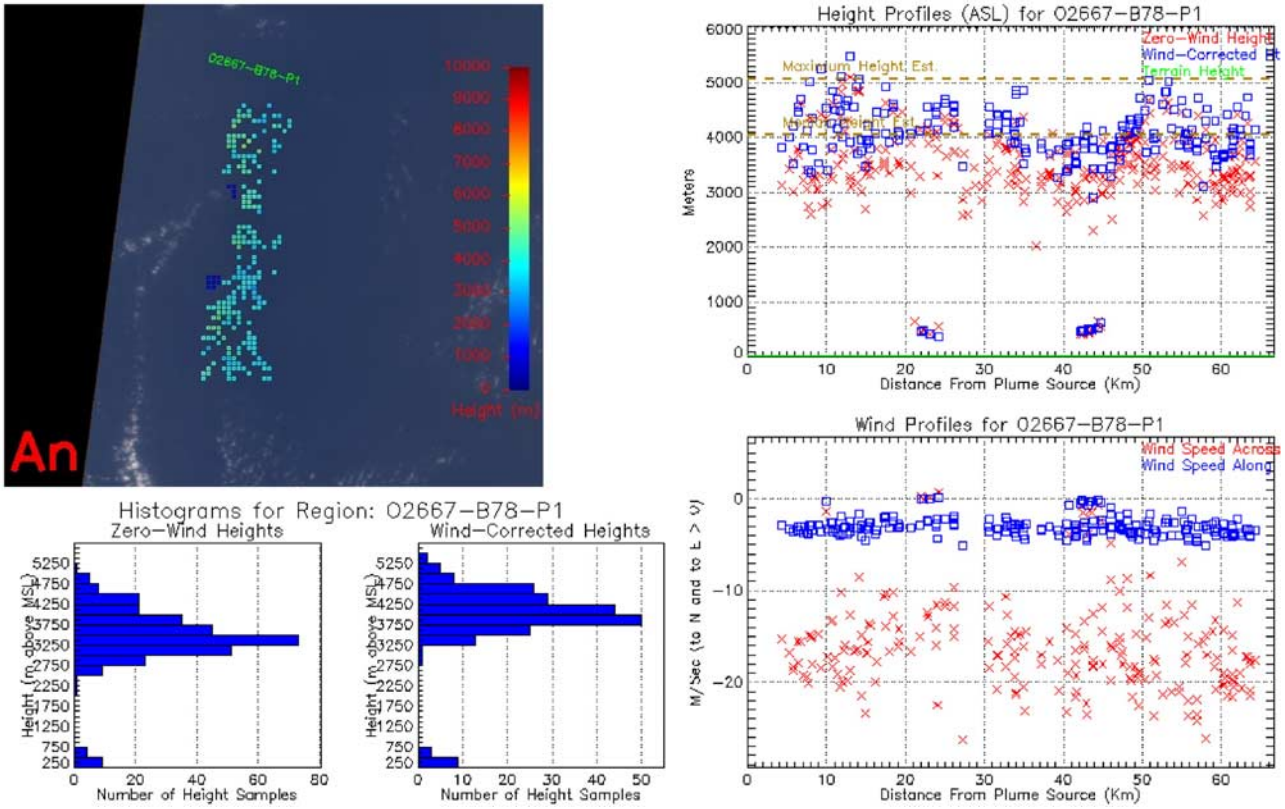

Figure 12. MISR stereo plume height retrievals over the ocean near Capo Verde on 18 June 2000 (MISR orbit 2667, block 78). (top left) Selected plume region, (bottom left) histograms of plume heights retrieved under zero-wind and nonzero-wind assumptions, (top right) MISR-retrieved height profiles (the distance from plume source is defined as distance from the first selected pixel in the image), and (bottom right) MISR-retrieved wind profiles.

over remote areas where heavy dust loading frequently occurs will require additional data from the AIRS, CALIPSO and OMI sensors and transport model simulations.

[36] **Acknowledgments.** We thank Michael Garay for creating tools for collocating MISR and MODIS aerosol retrievals; Amy Braverman, PI of AMAPS project, for her help in developing tools for obtaining and comparing MISR, MODIS, and AERONET data; and the AERONET project and the Saharan AERONET stations principal investigators for their efforts in establishing and maintaining the nine sites used in this investigation. We thank Jeffrey Reid and Douglas Westphal for sharing NAAPS data and the MISR team for providing facilities, access to data, and useful discussions. The work of O. Kalashnikova is supported by a grant from the NASA Earth Sciences Division, Climate and Radiation program, under H. Maring. The work of R. Kahn is supported in part by the NASA Climate and Radiation Research and Analysis program under H. Maring, the Atmospheric Composition program under Phil DeCola, and the EOS-MISR instrument project. This work was performed at the Jet Propulsion Laboratory, California Institute of Technology, under contract with NASA and at the NASA Goddard Space Flight Center. The MISR data were obtained from the NASA Langley Research Center Atmospheric Sciences Data Center.

References

Bopp, L., K. E. Kohfeld, C. Le Quéré, and O. Aumont (2003), Dust impact on marine biota and atmospheric CO2 during glacial periods, *Paleoceanography*, *18*(2), 1046, doi:10.1029/2002PA000810.

Chen, W.-T., R. A. Kahn, D. Nelson, K. Yau, and J. H. Seinfeld (2008), Sensitivity of multiangle imaging to the optical and microphysical properties of biomass burning aerosols, *J. Geophys. Res.*, *113*, D10203, doi:10.1029/2007JD009414.

Chiapello, I., C. Moulin, and J. M. Prospero (2005), Understanding the long-term variability of African dust transport across the Atlantic as recorded in both Barbados surface concentrations and large-scale Total Ozone Mapping Spectrometer (TOMS) optical thickness, *J. Geophys. Res.*, *110*, D18S10, doi:10.1029/2004JD005132.

Christensen, J. H. (1997), The Danish eulerian hemispheric model—A three-dimensional air pollution model used for the Arctic, *Atmos. Environ.*, *31*, 4169–4191, doi:10.1016/S1352-2310(97)00264-1.

Christopher, S., and J. Wang (2004), Inter-comparison between MISR and Sunphotometer AOT in dust Source Regions over China: Implications to satellite retrievals and radiative forcing calculations, *Tellus, Ser. B*, *56*(5), 451–456, doi:10.1111/j.1600-0889.2004.00120.x.

Colarco, P. R., et al. (2003), Saharan dust transport to the Caribbean during PRIDE: 2. Transport, vertical profiles, and deposition in simulations of in situ and remote sensing observations, *J. Geophys. Res.*, *108*(D19), 8590, doi:10.1029/2002JD002659.

DeSouza-Machado, S. G., L. L. Strow, S. E. Hannon, and H. E. Motteler (2006), Infrared dust spectral signatures from AIRS, *Geophys. Res. Lett.*, *33*, L03801, doi:10.1029/2005GL024364.

Diner, D. J., et al. (2001), MISR level 2 aerosol retrieval algorithm theoretical basis, rev. E, *JPL-D11400*, Jet Propul. Lab., Pasadena, Calif.

Dubovik, O., A. Smirnov, B. N. Holben, M. D. King, Y. J. Kaufman, T. F. Eck, and I. Slutsker (2000), Accuracy assessments of aerosol optical properties retrieved from AERONET sun and sky-radiance measurements, *J. Geophys. Res.*, *105*, 9791–9806.

Evan, A. T., J. Dunion, J. A. Foley, A. K. Heidinger, and C. S. Velden (2006), New evidence for a relationship between Atlantic tropical cyclone activity and African dust outbreaks, *Geophys. Res. Lett.*, *33*, L19813, doi:10.1029/2006GL026408.

Ginoux, P., and O. Torres (2003), Empirical TOMS index for dust aerosol: Applications to model validation and source characterization, *J. Geophys. Res.*, *108*(D17), 4534, doi:10.1029/2003JD003470.

Gu, G., R. F. Adler, G. J. Huffman, and S. Curtis (2004), African easterly waves and their association with precipitation, *J. Geophys. Res.*, *109*, D04101, doi:10.1029/2003JD003967.

Hogan, T. F., and L. R. Brody (1993), Sensitivity studies of the Navy's global forecast model parameterizations and evaluation of improvements

to NOGAPS, *Mon. Weather Rev.*, *121*, 2373–2395, doi:10.1175/1520-0493(1993)121<2373:SSOTNG>2.0.CO;2.

Hogan, T. F., and T. E. Rosmond (1991), The description of the Navy operational global atmospheric prediction system's spectral forecast model, *Mon. Weather Rev.*, *119*, 1786–1815, doi:10.1175/1520-0493(1991)119<1786:TDOTNO>2.0.CO;2.

Holben, B. N., et al. (1998), AERONET - A federated instrument network and data archive for aerosol characterization, *Remote Sens. Environ.*, *66*(1), 1–16, doi:10.1016/S0034-4257(98)00031-5.

Holben, B., et al. (2001), An emerging ground based aerosol climatology: Aerosol optical depth from AERONET, *J. Geophys. Res.*, *106*, 12,067–12,097, doi:10.1029/2001JD900014.

Huang, J., P. Minnis, Y. Yi, Q. Tang, X. Wang, Y. Hu, Z. Liu, K. Ayers, C. Trepte, and D. Winker (2007), Summer dust aerosols detected from CALIPSO over the Tibetan Plateau, *Geophys. Res. Lett.*, *34*, L18805, doi:10.1029/2007GL029938.

Jones, C., N. Mahowald, and C. Luo (2004), Observational evidence of African desert dust intensification of easterly waves, *Geophys. Res. Lett.*, *31*, L17208, doi:10.1029/2004GL020107.

Kahn, R., R. West, D. McDonald, B. Rheingans, and M. Mishchenko (1997), Sensitivity of Multi-angle remote sensing observations to aerosol sphericity, *J. Geophys. Res.*, *102*, 16,861–16,870, doi:10.1029/96JD01934.

Kahn, R., P. Banerjee, D. McDonald, and D. Diner (1998), Sensitivity of multiangle imaging to aerosol optical depth and a pure size distribution and composition over ocean, *J. Geophys. Res.*, *103*, 32,195–32,213, doi:10.1029/98JD01752.

Kahn, R., P. Banerjee, and D. McDonald (2001), The sensitivity of multi-angle imaging to natural mixtures of aerosols over ocean, *J. Geophys. Res.*, *106*, 18,219–18,238, doi:10.1029/2000JD900497.

Kahn, R., B. Gaitley, J. Martonchik, D. Diner, K. Crean, and B. Holben (2005), MISR global aerosol optical depth validation based on two years of coincident AERONET observations, *J. Geophys. Res.*, *110*, D10S04, doi:10.1029/2004JD004706.

Kahn, R. A., W.-H. Li, C. Moroney, D. J. Diner, J. V. Martonchik, and E. Fishbein (2007a), Aerosol source plume physical characteristics from space-based multiangle imaging, *J. Geophys. Res.*, *112*, D11205, doi:10.1029/2006JD007647.

Kahn, R. A., M. J. Garay, D. L. Nelson, K. K. Yau, M. A. Bull, B. J. Gaitley, J. V. Martonchik, and R. C. Levy (2007b), Satellite-derived aerosol optical depth over dark water from MISR and MODIS: Comparisons with AERONET and implications for climatological studies, *J. Geophys. Res.*, *112*, D18205, doi:10.1029/2006JD008175.

Kalashnikova, O. V., and R. Kahn (2006), Ability of multiangle remote sensing observations to identify and distinguish mineral dust types: Sensitivity over dark water, *J. Geophys. Res.*, *111*, D11207, doi:10.1029/2005JD006756.

Kalashnikova, O. V., R. Kahn, I. N. Sokolik, and W.-H. Li (2005), The ability of multi-angle remote sensing observations to identify and distinguish mineral dust types: 1. Optical models and retrievals of optically thick plumes, *J. Geophys. Res.*, *110*, D18S14, doi:10.1029/2004JD004550.

Kaufman, Y. J., I. Koren, L. A. Remer, D. Tanré, P. Ginoux, and S. Fan (2005), Dust transport and deposition observed from the Terra-Moderate Resolution Imaging Spectroradiometer (MODIS) spacecraft over the Atlantic Ocean, *J. Geophys. Res.*, *110*, D10S12, doi:10.1029/2003JD004436.

Mahowald, N., C. Luo, J. del Corral, and C. S. Zender (2003), Interannual variability in atmospheric mineral aerosols from a 22-year model simulation and observational data, *J. Geophys. Res.*, *108*(D12), 4352, doi:10.1029/2002JD002821.

Mahowald, N. M., A. R. Baker, G. Bergametti, N. Brooks, R. A. Duce, T. D. Jickells, N. Kubilay, J. M. Prospero, and I. Tegen (2005), Atmospheric global dust cycle and iron inputs to the ocean, *Global Biogeochem. Cycles*, *19*, GB4025, doi:10.1029/2004GB002402.

Martin, J. H., S. E. Fitzwater, and R. M. Gordon (1991), We still say iron deficiency limits phytoplankton growth in the Subarctic Pacific, *J. Geophys. Res.*, *96*(C11), 20,699–20,700, doi:10.1029/91JC01935.

Martonchik, J. V., D. J. Diner, R. Kahn, B. Gaitley, and B. N. Holben (2004), Comparison of MISR and AERONET aerosol optical depths over desert sites, *Geophys. Res. Lett.*, *31*, L16102, doi:10.1029/2004GL019807.

Mishchenko, M. I., I. V. Geogdzhayev, B. Cairns, B. E. Carlson, J. Chowdhary, A. A. Lacis, L. Liu, W. B. Rossow, and L. D. Travis (2007), Past, present, and future of global aerosol climatologies derived from satellite observations: A perspective, *J. Quant. Spectrosc. Radiat. Transfer*, *106*, 325–347, doi:10.1016/j.jqsrt.2007.01.007.

Pierangelo, C., A. Chédin, S. Heilliette, N. Jacquinet-Husson, and R. Armante (2004), Dust altitude and infrared optical depth from AIRS, *Atmos. Chem. Phys.*, *4*, 1823–1836, sref:1680-7324/acp/2004-4-1823.

Pierangelo, C., M. Mishchenko, Y. Balkanski, and A. Chédin (2005), Retrieving the effective radius of Saharan dust coarse mode from AIRS, *Geophys. Res. Lett.*, *32*, L20813, doi:10.1029/2005GL023425.

Prospero, J. M., P. Ginoux, O. Torres, S. E. Nicholson, and T. E. Gill (2002), Environmental characterization of global sources of atmospheric soil dust identified with the NIMBUS 7 Total Ozone Mapping Spectrometer (TOMS) absorbing aerosol product, *Rev. Geophys.*, *40*(1), 1002, doi:10.1029/2000RG000095.

Reid, J. S., D. L. Westphal, J. M. Livingston, D. L. Savoie, H. B. Maring, H. H. Jonsson, D. P. Eleuterio, J. E. Kinney, and E. A. Reid (2002), Dust vertical distribution in the Caribbean during the Puerto Rico Dust Experiment, *Geophys. Res. Lett.*, *29*(7), 1151, doi:10.1029/2001GL014092.

Reid, J. S., et al. (2003), Analysis of measurements of Saharan dust by airborne and ground-based remote sensing methods during the Puerto Rico Dust Experiment (PRIDE), *J. Geophys. Res.*, *108*(D19), 8586, doi:10.1029/2002JD002493.

Remer, L. A., et al. (2005), The MODIS aerosol algorithm, products and validation, *J. Atmos. Sci.*, *62*(4), 947–973, doi:10.1175/JAS3385.1.

Shinn, E. A., G. W. Smith, J. M. Prospero, P. Betzer, M. L. Hayes, V. Garrison, and R. T. Barber (2000), African dust and the demise of Caribbean coral reefs, *Geophys. Res. Lett.*, *27*(19), 3029–3032, doi:10.1029/2000GL011599.

Tegen, I., and R. Miller (1998), A general circulation model study on the interannual variability of soil dust aerosol, *J. Geophys. Res.*, *103*(D20), 25,975–25,996, doi:10.1029/98JD02345.

Torres, O., P. K. Bhartia, J. R. Herman, Z. Ahmad, and J. Gleason (1998), Derivation of aerosol properties from satellite measurements of backscattered ultraviolet radiation: Theoretical basis, *J. Geophys. Res.*, *103*(D14), 17,099–17,110, doi:10.1029/98JD00900.

Torres, O., A. Tanskanen, B. Veihelmann, C. Ahn, R. Braak, P. K. Bhartia, P. Veefkind, and P. Levelt (2007), Aerosols and surface UV products from Ozone Monitoring Instrument observations: An overview, *J. Geophys. Res.*, *112*, D24S47, doi:10.1029/2007JD008809.

Vaughan, M. A., S. A. Young, D. M. Winker, K. A. Powell, A. H. Omar, Z. Liu, Y. Hu, and C. A. Hostetler (2004), Fully automated analysis of space-based lidar data: An overview of the CALIPSO retrieval algorithms and data products, *Proc. SPIE Int. Soc. Opt. Eng.*, *5575*, 16–30, doi:10.1117/12.572024.

Wang, Z., H. Akimoto, and I. Uno (2002), Neutralization of soil aerosol and its impact on the distribution of acid rain over east Asia: Observations and model results, *J. Geophys. Res.*, *107*(D19), 4389, doi:10.1029/2001JD001040.

Westphal, D. L., O. B. Toon, and T. N. Carlson (1988), A case study of mobilization and transport of Saharan dust, *J. Atmos. Sci.*, *45*, 2145–2175, doi:10.1175/1520-0469(1988)045<2145:ACSOMA>2.0.CO;2.

Wong, S., P. R. Colarco, and A. E. Dessler (2006), Principal component analysis of the evolution of the Saharan air layer and dust transport: Comparisons between a model simulation and MODIS and AIRS retrievals, *J. Geophys. Res.*, *111*, D20109, doi:10.1029/2006JD007093.

Wu, L. G. (2007), Impact of 5 Saharan air layer on hurricane peak intensity, *Geophys. Res. Lett.*, *34*, L09802, doi:10.1029/2007GL029564.

Yu, H., R. E. Dickinson, M. Chin, Y. J. Kaufman, B. N. Holben, I. V. Geogdzhayev, and M. I. Mishchenko (2003), Annual cycle of global distributions of aerosol optical depth from integration of MODIS retrievals and GOCART model simulations, *J. Geophys. Res.*, *108*(D3), 4128, doi:10.1029/2002JD002717.

Yu, H., et al. (2006), A review of measurement-based assessments of the aerosol direct radiative effect and forcing, *Atmos. Chem. Phys.*, *6*, 613–666.

R. A. Kahn, NASA Goddard Space Flight Center, Greenbelt, MD 20771, USA.

O. V. Kalashnikova, Jet Propulsion Laboratory, California Institute of Technology, Pasadena, CA 91109, USA. (olga.v.kalashnikova@jpl.nasa.gov)